Microstructural and mechanical properties of 17-4PH stainless steel fabricated via material extrusion 3D printing

Dang Long Cao[1], Van Cuong Nguyen [2*] and Van Nga Tran Thi [2]

[1] Department of Mechanical Engineering, Vinh Long University of Technology Education, **Vietnam**
[2] Department of Mechanical Engineering, University of Transport and Communications, **Vietnam**

* Corresponding Author: nguyencuong@utc.edu.vn
*Received:*18 April 2025; *1st Revised:* 11 May 2025; *2nd Revised*: 03 June 2025; *Accepted:* 07 June 2025

Cite this https://doi.org/10.24036/teknomekanik.v8i1.34872

Abstract: This study investigates the microstructural and mechanical properties of metal 3D printing products fabricated using material extrusion technology. It focuses on the critical post-processing stages: printing, washing, and sintering. A Markforged 3D printing system and 17-4 PH stainless steel material were utilized to assess the effect of printing orientation and sintering conditions on microstructural and mechanical properties of the final product. The results demonstrate that printing orientation and sintering conditions critically govern the microstructural and mechanical properties of the final product. During sintering, the microstructure undergoes significant phase transformation and densification, while micropores and shrinkage voids emerge due to capillary stresses during binder removal. Furthermore, the mechanical properties are significantly influenced by the combined effects of printing orientation and sintering conditions. Optimizing deposition parameters (printing orientations and sintering conditions) substantially enhances the mechanical performance of the final printed product.

Keywords: additive manufacturing; material extrusion technology; 3D Metal printing; microstructure

1. Introduction

Additive Manufacturing (AM), widely known as 3D printing, represents a significant advancement in modern manufacturing [1][2][3][4]. Emerged as a prominent manufacturing technique for engineering materials, including ceramics, polymers, and metals, due to its versatility and cost-effectiveness [5], [6], [7]. According to ISO/ASTM52900-15, 2015, metal 3D printing technologies are classified into seven categories: Material Extrusion (ME), Material Jetting (MJ), Binder Jetting (BJ), VAT Photopolymerization, Powder Bed Fusion (PBF), Direct Energy Deposition (DED), and Sheet Lamination. Among these, Material Extrusion (ME) technology represented approximately 10% of the global metal 3D printing market in 2020 [8], [9]. Material Extrusion (ME) technology is characterized by the layer-by-layer deposition of a metal-polymer composite filament through a heated nozzle to form the desired geometry [10], [11], [12], [13]. Unlike powder-based metal 3D printing technologies, ME employs material filaments comprising a mixture of metal powder and a polymer binder [14], [15]. The material extrusion process includes four main stages: (1) Material filaments fabrication, (2) Green-part printing, (3) Washing, and (4) Sintering [16], [17], [18]. Among these, material filaments fabrication plays a crucial role. It encompasses the selection of metal powder, binder composition, and additives to ensure final printed component quality. These filaments are fabricated by combining metal powder and polymer binder in precise ratios, which critically affect the mechanical performance [19]. Moreover, the quality of the metal powder critically governs both the filament characteristics and the properties of the final printed product [20], [21].

Despite significant process innovations, ME technology is hindered by persistent challenges in achieving consistent metallurgical quality in the final printed product. Comprehensive characterization of microstructural and mechanical performance is critical for optimizing manufacturing parameters and improving product quality [22], [23]. Key processing parameters (shrinkage, printing orientation, printing speed, and layer thickness) demonstrate a significant effect on the microstructural and mechanical performance of the final printed product [24], [25], [26]. Existing studies have assessed critical microstructural properties (particularly porosity and dimensional accuracy) and mechanical strength. Kurose et al. (2020) reported a 20% variation in mechanical strength between vertically and horizontally oriented 316L stainless steel components fabricated via Material Extrusion (ME), attributing this anisotropy primarily to insufficient interlayer bonding during the sintering process [24]. Caminero et al. (2021) quantified porosity in 316L stainless steel fabricated via fused filament fabrication, employing both Archimedes' method and micro-CT scanning. Their results demonstrated porosity variation of 1−5% depending on processing conditions [26].

Similarly, Tosto et al. (2022) examined the effect of layer height and infill pattern on dimensional shrinkage. Printing orientation significantly impacts the accuracy and tolerance of the final product [25]. These findings underscore the critical need to consider both printing orientation and post-processing steps, particularly the sintering process, when assessing the structural performance of ME-fabricated parts. Zhang et al. (2022) comprehensively reviewed advances in metal Material Extrusion (ME), identifying critical challenges in material preparation, printing accuracy, sintering densification, and mechanical anisotropy. Their study identifies that although ME is a promising low-cost alternative for fabricating complex metal components, issues such as residual porosity, layer adhesion, and dimensional shrinkage still require further investigation and optimization. These observations reinforce the relevance and necessity of the present study, which addresses several of these concerns through experimental evaluation of 17-4PH stainless steel samples across different process stages and orientations [27].

Thus, this study systematically investigates the microstructural and mechanical properties of 17-4PH stainless steel components fabricated via Material Extrusion (ME) technology using the Markforged Metal X system. Whereas existing studies primarily assessed the mechanical properties of ME-printed parts at a single post-processing stage. This study addresses the current critical gap by combining comprehensive microstructural characterization (via SEM and EDS) and mechanical testing across all manufacturing phases: green printing, washing, and sintering. It focuses on printing orientation and sintering conditions that enable the quantification of changes in elemental composition and porosity, as well as correlation with mechanical properties. By examining the interplay between printing orientation, microstructural, and anisotropic mechanical properties, this study improves the quality and structural integrity of ME-printed metal products, aligning with the stringent demands of advanced industrial applications.

2. Material and methods

2.1 Additive manufacturing

The experimental samples were printed in various directions to assess the microstructural and mechanical properties of the printed products. The material used for the Material Extrusion (ME) 3D printer was a composite consisting of 17–4 PH stainless steel and a polymer binder. The 17-4PH stainless steel is a precipitation-hardening martensitic stainless steel widely used in aerospace, automotive, and medical industries due to its high strength, excellent corrosion resistance, and good machinability [28], [29], [30], [31]. Its compatibility with heat treatment and potential for property optimization make it an ideal candidate for additive manufacturing processes, including

ME. The printed samples were prepared as tensile specimens manufactured using the Markforged Metal X 3D printing system with standard dimensions, as illustrated in Figure 1.

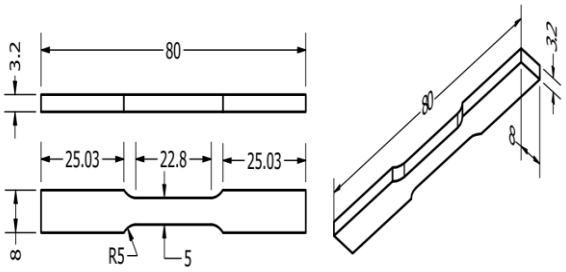

Figure 1. CAD model and dimensions of the 17-4PH stainless steel as a specimen for mechanical testing under the ASTM E8 standard

The CAD model data in .STL format is managed online by the user via the supplier's website, where model parameters such as material, model size, and position on the printing bed can be configured. The printing time and production cost of the model can be monitored and adjusted. All test specimens were printed under the same conditions and printing settings (Table 1). The composition of the 17-4 PH steel material is based on the datasheet from the supplier (Table 2).

Table 1. Printing parameters used for 17-4PH stainless steel samples in the material extrusion process

Materials	17-4PH Stainless Steel
Post-sinter layer height (mm)	0.125mm
Original units	Metric
Scale	0.4
Fill pattern	Triangular fill
Roof & floor layers	4
Wall layers	4

In the ME process, the printing filament consists of a binder material typically a thermoplastic and fine metal powder. This filament is heated and extruded through a circular nozzle (Figure 2), with the figure schematically illustrating the entire experimental workflow. The nozzle melts the filament to its softening point, allowing it to be extruded layer by layer to form the three-dimensional geometry. The surface quality of the printed object is relatively low due to the round shape of the nozzle and the spacing between layers. The printed object at this stage is known as the "green" part, which retains high porosity and contains a significant amount of polymer binder.

Table 2. The composition of 17–4 PH stainless steel

Composition	Amount
Chromium	15–17.5%
Nickel	3–5%
Copper	3–5%
Silicon	1% max
Manganese	1% max
Niobium	0.15–0.45%
Carbon	0.07%
Phosphorous	0.04% max
Sulfur	0.03% max
Iron	Balanced

After printing, the green part undergoes a two-step post-processing procedure: washing and sintering. All other process parameters were maintained constant and followed the default configuration provided by the Markforged Metal X system and Eiger software. The printed sample is allowed to cool for 30 minutes before being immersed in Opteon SF97 solvent within the immersion chamber. The solvent is pre-heated to its boiling point in the boiling chamber. During this process, heat promotes the removal of most of the wax and polymer binder. Once the washing process is complete, the sample is transferred to the drying chamber. The washing and drying durations depend on the shape, size, and material of the sample. The drying process eliminates residual solvent, preventing contamination that could compromise subsequent sintering. After drying, the sample is weighed to confirm sufficient mass loss (approximately 4.2%). Insufficient binder removal can compromise the sintering process, reduce part quality, or cause binder accumulation within the furnace. Therefore, the washing process is repeated if the mass loss is below 4.2%.

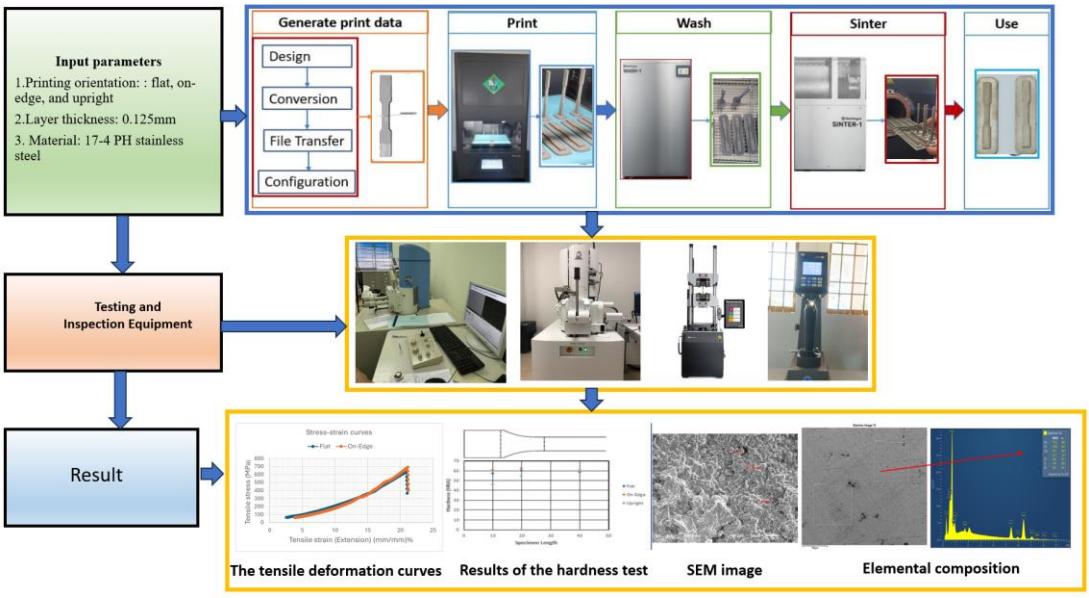

Figure 2. Experimental and evaluation workflow for 17-4PH stainless steel using the metal extrusion process

Sintering is employed to fuse metal powder particles. It fills the voids left by the polymer binder removed during the washing process, increasing the density of the product. The samples are loaded into the furnace with proper arrangement to prevent deformation or undesired interactions between parts during sintering. They are arranged with adequate spacing between them and do not overlap. The heat treatment is conducted in a non-pressure furnace and maintained at a maximum temperature below the melting point of the metal.

2.2 Characterization methods

The cross-sectional structures of the samples were analyzed using a JSM-6510LV scanning electron microscope (SEM). The printed samples were sectioned into smaller cross-sections using a wire cutter and embedded in a 25mm diameter round silicon mold filled with epoxy resin. After curing, the samples were ground and polished on their cross-sections using SiC sandpapers (grit size from #100 to #200). Subsequently, they were cleaned with pure ethanol. The prepared samples were then dried in a vacuum oven (50°C, 30 minutes) before capturing surface micrographs. The sample was characterized by its cross-sectional elemental composition using energy-dispersive X-ray spectroscopy (EDS) coupled with SEM JSM-IT800LV. Samples were collected at each stage of the process and analyzed using SEM to evaluate the layer arrangement, surface morphology, and cross-

sectional structure. The primary objectives of the analysis were to determine the powder particle size, assess porosity, and examine changes in material composition throughout the printing process.

The tensile strength testing is conducted using the 300DX Static Hydraulic Universal Testing Machine following the ASTM standard 8-08. Five samples from each printing orientation are tested for tensile strength, and the average values are obtained. Before testing, the samples were conditioned under controlled environmental (60–65% relative humidity, 27°C) for 48 hours. Hardness measurements were performed using a Wilson Hardness 574 Rockwell hardness tester. This instrument determines the surface strength of materials by measuring the depth of indentation under a specified load.

3. Results and discussion

3.1 Microstructure morphology

The microstructure morphology of the "green" state of the product at varying magnifications highlights the typical characteristics of the material post-printing (Figure 3). Metal powder particles are primarily bonded by a polymer binder, forming mechanical connections through the polymer coating. Numerous voids are observed, and the particles are not in full contact with one another. The grain structure appears rough, with a non-uniform surface texture. Particle sizes range from 2.4 µm to 4.2 µm, displaying a porous structure characteristic of the "green" state. At this stage, the product remains soft, prone to deformation, and easily breakable.

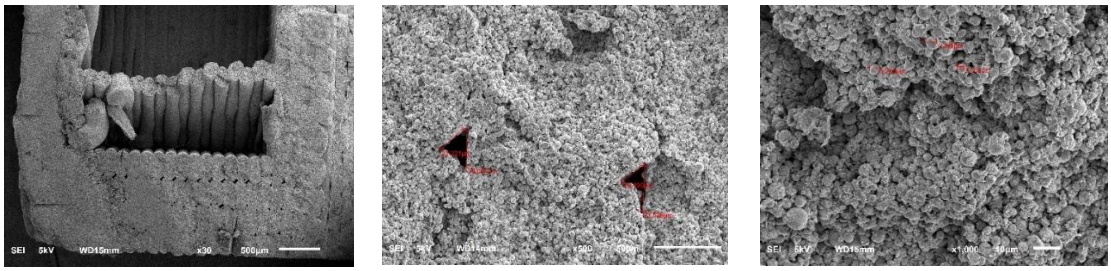

Figure 3. SEM images of the grain structure of the product in the green printing

After washing, the structure undergoes noticeable changes (Figure 4). The metal particles exhibit a size distribution of 1.6 µm to 2.2 µm, with the binder partially removed. It produces more loosely bound metal particles. Although less porous than the "green" state, significant voids persist between the particles due to the separated binder.

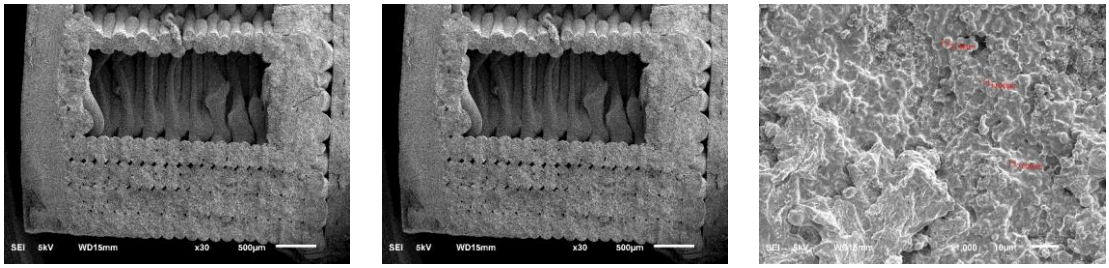

Figure 4. SEM image of the grain structure after the washing

The grain structure after sintering undergoes a significant transformation (Figure 5). The grains have coalesced into a cohesive solid mass, with a substantial reduction in pore size. Significant grain deformation has produced a smoother and denser surface morphology, indicating active recrystallization. High-temperature sintering induces grain rearrangement, forming a more

compact grain structure and increasing mechanical strength. Despite this, residual porosity (approximately 0.43%) persists with pore sizes ranging from 1 µm to 108 µm.

3.2 Elemental Composition Analysis (EDS)

In the "green" state (Figure 6), the printed sample has not yet undergone sintering; thus, the metal powder particles remain bonded by the polymer binder. EDS analysis shows a high carbon content (52.75%), as the polymer binder not only supplies carbon but also reduces the proportion of other metallic elements. The measured oxygen content of 2.625% principally derives from metal particles or from the binder itself. During printing and storage, metal particles are prone to oxidation and forming metal oxides on the surface. Iron (Fe) constitutes approximately 33.95% of the composition, with trace amounts of chromium (Cr), copper (Cu), and silicon (Si). These trace elements indicate residual support materials or contributions from the underlying substrate structure.

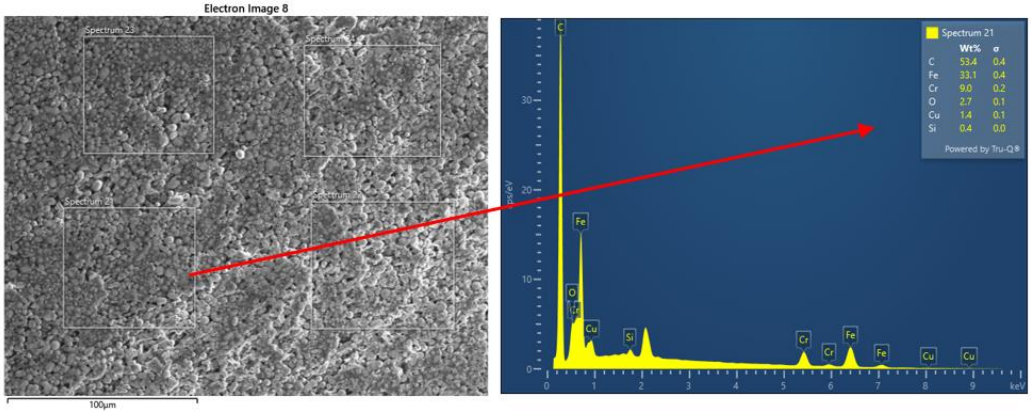

Figure 6. Elemental composition of the sample after printing

Washing removes residual binder and surface oxides (Figure 7), thereby increasing the overall carbon content within the sample. This process reduces the iron (Fe) content slightly to 27.2%, while carbon (C) increases significantly to an average of 60.5%. Washing exposes the sample to air and solvent, forming oxygen absorption and a thin oxide layer on the sample surface. Consequently, the oxygen (O) content increases from 2.625% (as printed state) to 3.15% (after washing). Concentrations of chromium (Cr), copper (Cu), and silicon (Si) decrease slightly, likely due to elemental dispersion or particle loss during washing, as these elements primarily comprise the protective oxide layer. Particularly, Cr decreases from 8.975% (in the printed state) to 7.75% (after washing), while Cu decreases from 1.4% to 1.2%.

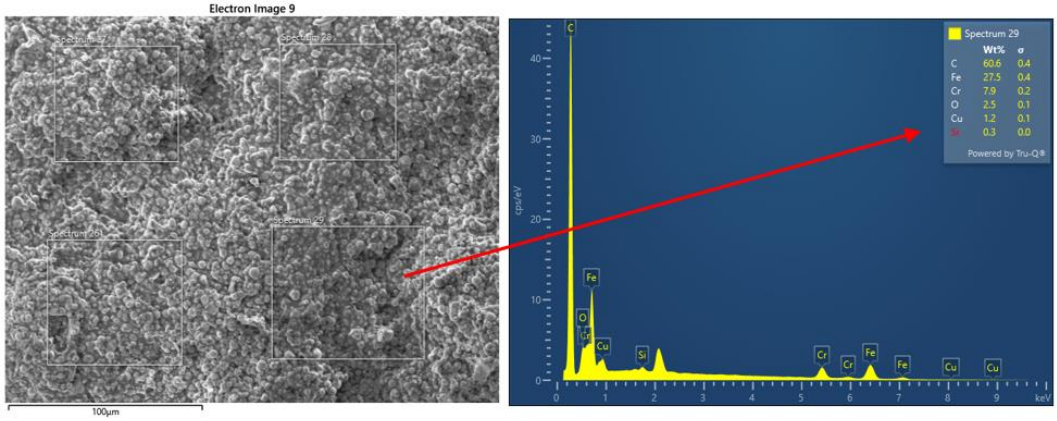

Figure 7. Elemental composition of the sample after washing

The sintering effectively removes most impurities, particularly residual carbon and surface oxides, thereby exposing the base metal structure and driving a significant increase in iron (Fe) content. The Fe mass fraction increased from an average of 27.75% (after washing) to 72.2% (after sintering), as shown in Figure 8. Sintering decomposed residual carbon (mainly polymer binder-derived). It decreases carbon content from 60.5% (after washing) to 2.66% (after sintering).

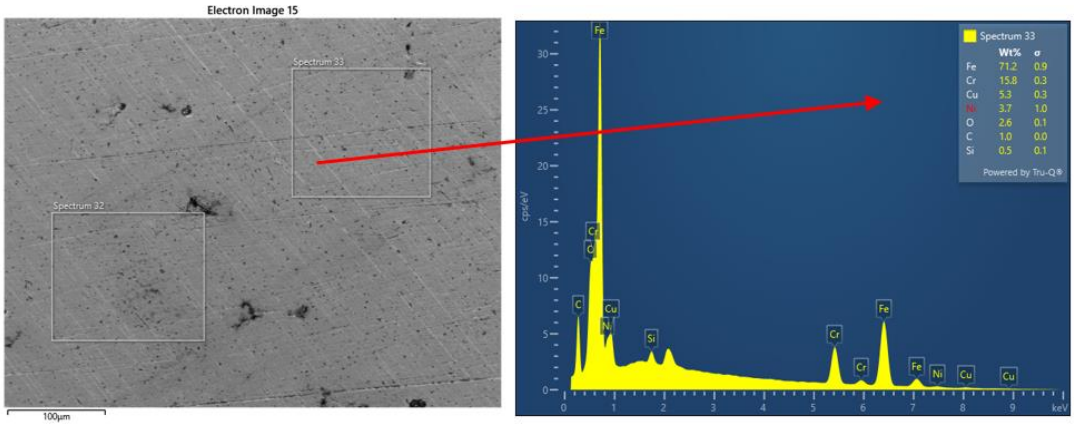

Figure 8. Elemental composition of the sample after sintering

Furthermore, the mass fractions of alloying elements (Cr, Ni, and Cu) increase significantly. Cr increases from 7.75% (after washing) to 15.37% (after sintering), Ni increases from 0% (after washing) to 3.41% (after sintering), and Cu increases from 1.2% (after washing) to 4.68% (after sintering). These changes in elemental composition reflect the structural transformation and densification during sintering, which play a crucial role in improving the mechanical properties and overall quality of the material. The EDS analysis results at the three stages: after printing, after washing, and after sintering, are detailed in Table 3.

Table 3. Mass fraction (wt%) of different measurement positions on the sample across three stages: after printing, after washing, and after sintering

Element (Wt%)	Cr	Ni	Cu	Si	Mn	C	P	S	O	Al	Fe
Print											
Spectrum 21	9	0	1.4	0.4	0	53.4	0	0	2.7	0	33.1
Spectrum 22	9.4	0	1.4	0.3	0	50.5	0	0	2.7	0	35.8
Spectrum 23	8.3	0	1.5	0.3	0	55.8	0	0	2.4	0	31.7
Spectrum 24	9.2	0	1.3	0.3	0	51.3	0	0	2.7	0	35.2
AVERAGE	8.975	0	1.4	0.325	0	52.75	0	0	2.625	0	33.95
Wash											
Spectrum 26	7.8	0	1.2	0.3	0	59.8	0	0	3.2	0	27.8
Spectrum 27	8.1	0	1.1	0.4	0	58.4	0	0	3.3	0	28.6
Spectrum 28	7.2	0	0.9	0.3	0	63.2	0	0	3.6	0	24.9
Spectrum 29	7.9	0	1.2	0.3	0	60.6	0	0	2.5	0	27.5
AVERAGE	7.75	0	1.1	0.325	0	60.5	0	0	3.15	0	27.2
Sinter											
Spectrum 28	15.0	3.8	4.9	1.1	0	1.4	0	0	3.7	0.4	69.0

Element (Wt%)	Cr	Ni	Cu	Si	Mn	C	P	S	O	Al	Fe
Spectrum 29	14.9	5.3	5.2	0.6	0	0.9	0	0	2.5	0	70.6
Spectrum 30	14.6	5.0	5.4	0.5	0	1.0	0	0	2.6	0	71.0
Spectrum 31	15.9	0	3.1	0.6	0	1.1	0	0	2.9	0	76.5
Spectrum 32	15.9	0	3.2	0.6	0	0.9	0	0	2.4	0	77.0
Spectrum 33	15.8	3.7	5.3	0.5	0	1.0	0	0	2.6	0	71.2
Spectrum 34	14.7	4.6	4.9	0.5	0	1.0	0	0	2.6	0.2	71.6
Spectrum 35	15.5	3.7	5.1	0.6	0	0.8	0	0	2.2	0	72.0
Spectrum 36	16.5	0	3.1	0.6	0	1.0	0	0	2.7	0	76.1
Spectrum 37	15.2	4.5	5.4	0.5	0	1.1	0	0	3.0	0.3	70.1
Spectrum 38	15.0	4.9	5.4	0.4	0	0.9	0	0	2.3	0.2	70.9
Spectrum 39	15.4	5.4	5.1	0.5	0	0.9	0	0	2.4	0	70.4
AVERAGE	15.37	3.41	4.68	0.58	0.00	1.00	0.00	0.00	2.66	0.28	72.20

3.3 Mechanical properties

The Rockwell hardness testing was performed at three points per specimen. Average hardness was 58.5HRA (flat direction) and 61.05 HRA (on edge direction). Specimens printed in the On-Edge orientation exhibited the highest hardness (61.05 HRA) due to their layer arrangement. Layers are perpendicular to the load direction during testing. This arrangement enhanced inter-layer overlap and bond density while reducing structural weak points. The observed differences in tensile strength among the samples printed in various orientations can be attributed to variations in interlayer bonding quality and load distribution. On-Edge orientation specimens exhibited an approximate 9% greater ultimate tensile strength (691 MPa) than Flat orientation specimens (630 MPa). Moreover, On-Edge orientation specimens exhibited higher elongation at break (21.24%) than Flat orientation specimens (21.05%).

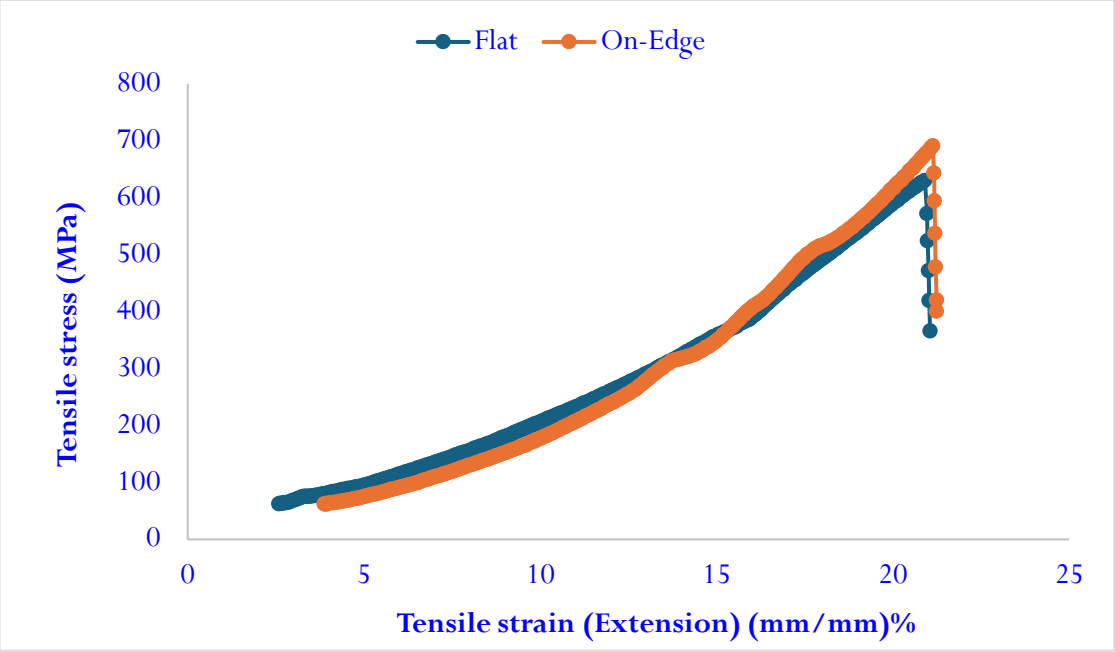

Figure 9. The tensile deformation curves

The On-Edge configuration enhanced tensile strength primarily due to the printed layers being stacked perpendicular to the loading direction. It facilitates more efficient stress transfer along continuous filament paths and minimizes weak interfacial effects. This orientation also improved interlayer diffusion and metallurgical bonding during the sintering, strengthening cohesion and overall mechanical properties. These results align with Kurose et al. [24], who observed similar improvements in mechanical properties for 316L stainless steel parts printed in optimized orientations.

The measured porosity level of the sintered samples was approximately 0.43%, which is relatively low and indicates effective densification during sintering. Compared to previous studies, this porosity is within or even below the typical range for metal parts produced using Material Extrusion (ME) technology. Caminero et al. [15] reported 1 to 5% porosity in 316L stainless steel fabricated via fused filament fabrication, varying with sintering condition and orientation. Likewise, Tosto et al. [25] observed porosity levels between 0.8% and 2.6% in ME-printed metal parts. The significantly lower porosity in the present study suggests optimized process control and favorable sintering conditions for 17-4PH stainless steel.

The densification behavior can be further explained by sintering theory. During sintering, the removal of binders combined with elevated temperatures promotes atomic diffusion. It drives particle bonding, pore shrinkage, and grain coalescence. Removal of polymeric binders and volatile components (causing approximately 4.2% mass loss) is a critical step to enable proper neck formation and diffusion bonding between adjacent metal particles. Diffusion-controlled sintering mechanisms govern porosity reduction and smooth grain boundary formation. It was confirmed by SEM micrographs in 17-4PH stainless steel. Volume and grain boundary diffusion dominate at sintering temperatures. Fe content increased from 27.2% to 72.2%, while carbon content decreased from 60.5% to 1.0% (EDS analysis), further validating the effectiveness of binder removal and metallurgical consolidation. These observations align with classical models of solid-state sintering. The sintering conditions applied in this study significantly enhance microstructural and mechanical properties.

4. Conclusion

This study presented a comprehensive investigation of the microstructural and mechanical properties of 17-4PH stainless steel components fabricated using Material Extrusion (ME) 3D printing technology. Through sequential analyses across green printing, washing, and sintering, this study revealed significant microstructural transformations and their correlation with mechanical properties. SEM and EDS analyses confirmed the effective removal of binder and redistribution of elemental composition during sintering. Particularly, increased Fe content, decreased C content, and porosity indicate substantial densification and metallurgical bonding. Printing orientation and sintering conditions influenced microstructural and mechanical properties. The study highlights the critical effects of printing orientation and sintering conditions. Future studies should optimize multi-parameter settings involving infill density, layer thickness, and sintering profiles to enhance part quality for stringent industrial applications.

Author's declaration

Author contribution

All authors contributed to the conception and design. The first draft of the manuscript was written by **Cao Dang Long** and **Nguyen Van Cuong**, and all authors commented on previous versions of the manuscript. **Nguyen Van Cuong** and **Tran Van Nga** provided valuable input, revisions, and feedback during manuscript development.

Funding statement

This research is funded by University of Transport and Communications (UTC) under grant number T2025-CK-002TĐ.

Data Availability

The datasets generated and analyzed during the current study—including microstructure morphology, elemental composition analysis, tensile strengt, and hardness—are not publicly available due to storage limitations but are available from the corresponding author upon reasonable request. All data are securely archived and can be provided to support transparency and reproducibility.

Acknowledgement

The authors would like to thank the governance of Vinh Long University of Technology Education and the University of Transport and Communications for their supports in providing equipment and materials necessary for conducting the experiments and completing this research. The authors also acknowledge the technical assistance provided by the laboratory staff of both institutions.

Competing interest

The authors declare no competing interest.

Ethical clearance

This research did not involve human or animal subjects.

AI statement

This article is the author's original work, written from original research, and no sections or figures were generated by AI.

Publisher's and Journal's note

Universitas Negeri Padang as the publisher, and Editor of Teknomekanik state that there is no conflict of interest towards this article publication.

References

[1] M. Armstrong, H. Mehrabi, and N. Naveed, "An overview of modern metal additive manufacturing technology," *J Manuf Process*, vol. 84, pp. 1001–1029, Dec. 2022, https://doi.org/10.1016/j.jmapro.2022.10.060

[2] R. Citarella and V. Giannella, "Additive Manufacturing in Industry," *Applied Sciences*, vol. 11, no. 2, p. 840, Jan. 2021, https://doi.org/10.3390/app11020840

[3] D. G. Zisopol, M. Minescu, and D. V. Iacob, "A Theoretical-Experimental Study on the Influence of FDM Parameters on the Dimensions of Cylindrical Spur Gears Made of PLA," *Engineering, Technology & Applied Science Research*, vol. 13, no. 2, pp. 10471–10477, Apr. 2023, https://doi.org/10.48084/etasr.5733

[4] D. G. Zisopol, I. Nae, A. I. Portoaca, and I. Ramadan, "A Statistical Approach of the Flexural Strength of PLA and ABS 3D Printed Parts," *Engineering, Technology & Applied Science Research*, vol. 12, no. 2, pp. 8248–8252, Apr. 2022, https://doi.org/10.48084/etasr.4739

[5] D. Anggara, R. Rifelino, Z. Abadi, and A. Arafat, "Exploring how 3D printing parameters affect the flexural strength of ABS materials," *Innovation in Engineering*, vol. 1, no. 2, pp. 125–133, Sep. 2024, https://doi.org/10.58712/ie.v1i2.16

[6] R. Citarella and V. Giannella, "Additive Manufacturing in Industry," *Applied Sciences*, vol. 11, no. 2, p. 840, Jan. 2021, https://doi.org/10.3390/app11020840

[7] K. V. Wong and A. Hernandez, "A Review of Additive Manufacturing," *ISRN Mechanical Engineering*, vol. 2012, pp. 1–10, Aug. 2012, https://doi.org/10.5402/2012/208760

[8] D. G. Zisopol, I. Nae, A. I. Portoaca, and I. Ramadan, "A Statistical Approach of the Flexural Strength of PLA and ABS 3D Printed Parts," *Engineering, Technology & Applied Science Research*, vol. 12, no. 2, pp. 8248–8252, Apr. 2022, https://doi.org/10.48084/etasr.4739

[9] Kianian B, " Wohlers Report 2019: 3D Printing and Additive Manufacturing State of the Industry, Annual Worldwide Progress Report : Chapter title: Middle East: Iran. Wohlers Report 2019 . 24. ed. FORT COLLINS, COLORADO, USA : Wohlers Associates, Inc., 2019," 2019.

[10] S. Spiller, F. Berto, and N. Razavi, "Mechanical behavior of Material Extrusion Additive Manufactured components: an overview," *Procedia Structural Integrity*, vol. 41, pp. 158–174, 2022, https://doi.org/10.1016/j.prostr.2022.05.018

[11] J. Vetter, F. Huber, S. Wachter, C. Körner, and M. Schmidt, "Development of a Material Extrusion Additive Manufacturing Process of 1.2083 steel comprising FFF Printing, Solvent and Thermal Debinding and Sintering," *Procedia CIRP*, vol. 113, pp. 341–346, 2022, https://doi.org/10.1016/j.procir.2022.09.140

[12] L. M. Galantucci, A. Pellegrini, M. G. Guerra, and F. Lavecchia, "3D Printing of parts using metal extrusion: an overview of shaping debinding and sintering technology," *Advanced Technologies & Materials*, vol. 47, no. 1, pp. 25–32, Jun. 2022, https://doi.org/10.24867/ATM-2022-1-005

[13] A. Kasha, S. O. Obadimu, and K. I. Kourousis, "Flexural characteristics of material extrusion steel 316L: Influence of manufacturing parameters," *Additive Manufacturing Letters*, vol. 3, p. 100087, Dec. 2022, https://doi.org/10.1016/j.addlet.2022.100087

[14] C. Van Nguyen, L. C. Dang, A. H. Le, and D. T. Bui, "A Study on the Influence of Printing Orientation in Metal Printing Using Material Extrusion Technology on the Mechanical Properties of 17-4 Stainless Steel Products," *Journal of Machine Engineering*, Aug. 2023, https://doi.org/10.36897/jme/170509

[15] C. N. Van, A. Le Hoang, C. D. Long, and D. N. Hoang, "Surface Roughness in Metal Material Extrusion 3D Printing: The Influence of Printing Orientation and the Development of a Predictive Model," *Engineering, Technology & Applied Science Research*, vol. 13, no. 5, pp. 11672–11676, Oct. 2023, https://doi.org/10.48084/etasr.6162

[16] M. Tebianian *et al.*, "A Review on the Metal Additive Manufacturing Processes." Aug. 02, 2023. https://doi.org/10.20944/preprints202308.0173.v1

[17] M. Nabipour, B. Akhoundi, and A. Bagheri Saed, "Manufacturing of polymer/metal composites by fused deposition modeling process with polyethylene," *J Appl Polym Sci*, vol. 137, no. 21, Jun. 2020, https://doi.org/10.1002/app.48717

[18] T. V. N. Tran, D. C. Long, and C. N. Van, "The Influence of Printing Materials on Shrinkage Characterization in Metal 3D Printing using Material Extrusion Technology," *Engineering, Technology & Applied Science Research*, vol. 14, no. 4, pp. 15356–15360, Aug. 2024, https://doi.org/10.48084/etasr.7758

[19] J. Costa, E. Sequeiros, M. T. Vieira, and M. Vieira, "Additive Manufacturing," *U.Porto Journal of Engineering*, vol. 7, no. 3, pp. 53–69, Apr. 2021, https://doi.org/10.24840/2183-6493_007.003_0005

[20] S. Singh, C. Prakash, P. Antil, R. Singh, G. Królczyk, and C. I. Pruncu, "Dimensionless Analysis for Investigating the Quality Characteristics of Aluminium Matrix Composites Prepared through Fused Deposition Modelling Assisted Investment Casting," *Materials*, vol. 12, no. 12, p. 1907, Jun. 2019, https://doi.org/10.3390/ma12121907

[21] A. Royer, T. Barrière, and J.-C. Gelin, "Development and Characterization of a Metal Injection Molding Bio Sourced Inconel 718 Feedstock Based on Polyhydroxyalkanoates," *Metals (Basel)*, vol. 6, no. 4, p. 89, Apr. 2016, https://doi.org/10.3390/met6040089

[22] J. Jacob, D. Pejak Simunec, A. E. Z. Kandjani, A. Trinchi, and A. Sola, "A Review of Fused Filament Fabrication of Metal Parts (Metal FFF): Current Developments and Future Challenges," *Technologies (Basel)*, vol. 12, no. 12, p. 267, Dec. 2024, https://doi.org/10.3390/technologies12120267

[23] A. Pellegrini, F. Lavecchia, M. G. Guerra, and L. M. Galantucci, "Influence of aging treatments on 17–4 PH stainless steel parts realized using material extrusion additive manufacturing technologies," *The International Journal of Advanced Manufacturing Technology*, vol. 126, no. 1–2, pp. 163–178, 2023, https://doi.org/10.1007/s00170-023-11136-3

[24] T. Kurose *et al.*, "Influence of the Layer Directions on the Properties of 316L Stainless Steel Parts Fabricated through Fused Deposition of Metals," *Materials*, vol. 13, no. 11, p. 2493, May 2020, https://doi.org/10.3390/ma13112493

[25] C. Tosto, J. Tirillò, F. Sarasini, C. Sergi, and G. Cicala, "Fused Deposition Modeling Parameter Optimization for Cost-Effective Metal Part Printing," *Polymers (Basel)*, vol. 14, no. 16, p. 3264, Aug. 2022, https://doi.org/10.3390/polym14163264

[26] M. Á. Caminero, A. Romero, J. M. Chacón, P. J. Núñez, E. García-Plaza, and G. P. Rodríguez, "Additive manufacturing of 316L stainless-steel structures using fused filament fabrication technology: mechanical and geometric properties," *Rapid Prototyp J*, vol. 27, no. 3, pp. 583–591, Apr. 2021, https://doi.org/10.1108/RPJ-06-2020-0120

[27] W. Cui, Y. Yang, L. Di, and F. Dababneh, "Additive manufacturing-enabled supply chain: Modeling and case studies on local, integrated production-inventory-transportation structure," *Addit Manuf*, vol. 48, p. 102471, Dec. 2021, https://doi.org/10.1016/j.addma.2021.102471

[28] G. Singh, J.-M. Missiaen, D. Bouvard, and J.-M. Chaix, "Additive manufacturing of 17–4 PH steel using metal injection molding feedstock: Analysis of 3D extrusion printing, debinding and sintering," *Addit Manuf*, vol. 47, p. 102287, Nov. 2021, https://doi.org/10.1016/j.addma.2021.102287

[29] C. Quinard, J. Song, T. Barriere, and J. C. Gelin, "Elaboration of PIM feedstocks with 316L fine stainless steel powders for the processing of micro-components," *Powder Technol*, vol. 208, no. 2, pp. 383–389, Mar. 2011, https://doi.org/10.1016/j.powtec.2010.08.033

[30] K. C. Tam, S. P. Yap, M. L. Foong, and N. H. Loh, "Metal injection molding: effects of the vinyl acetate content on binder behavior," *J Mater Process Technol*, vol. 67, no. 1–3, pp. 120–125, May 1997, https://doi.org/10.1016/S0924-0136(96)02830-0

[31] M. Chemkhi, J. M. Djouda, M. A. Bouaziz, J. Kauffmann, F. Hild, and D. Retraint, "Effects of Mechanical Post-Treatments on Additive Manufactured 17-4PH Stainless Steel Produced by Bound Powder Extrusion," *Procedia CIRP*, vol. 104, pp. 957–961, 2021, https://doi.org/10.1016/j.procir.2021.11.161